

THE EFFECT OF MAGNETIC SPOTS ON STELLAR WINDS AND ANGULAR MOMENTUM LOSS

O. COHEN¹, J. J. DRAKE¹, V. L. KASHYAP¹, AND T. I. GOMBOSI²

¹ Harvard-Smithsonian Center for Astrophysics, 60 Garden St., Cambridge, MA 02138, USA

² Center for Space Environment Modeling, University of Michigan, 2455 Hayward St., Ann Arbor, MI 48109, USA

Received 2009 March 23; accepted 2009 May 12; published 2009 June 23

ABSTRACT

We simulate the effect of latitudinal variations in the location of star spots, as well as their magnetic field strength, on stellar angular momentum loss (AML) to the stellar wind. We use the Michigan solar corona global magnetohydrodynamic model, which incorporates realistic relation between the magnetic field topology and the wind distribution. We find that the spots’ location significantly affects the stellar wind structure, and as a result, the total mass loss rate and AML rate. In particular, we find that the AML rate is controlled by the mass flux when spots are located at low latitudes but is controlled by an increased plasma density between the stellar surface and the Alfvén surface when spots are located at high latitudes. Our results suggest that there might be a feedback mechanism between the magnetic field distribution, wind distribution, AML through the wind, and the motions at the convection zone that generate the magnetic field. This feedback might explain the role of coronal magnetic fields in stellar dynamos.

Key words: methods: numerical – MHD – stars: coronae – stars: mass loss – stars: spots

Online-only material: color figures, extended figures

1. INTRODUCTION

Angular momentum loss (AML) through a magnetized wind can play a significant role in stellar evolution. It has been used to explain a number of stellar phenomena such as the evolution of close binaries and cataclysmic variables (CVs), evolution of stellar rotation rates, and dynamo saturation (e.g., Ivanova & Taam 2003, and references therein).

The principle mechanism by which the wind carries out angular momentum from the rotating object is as follows. The magnetic field is tangled to the surface of the star at one end but its other end is opened by the frozen-in wind at the point where the flow becomes super-Alfvénic (hereafter referred to in three dimensions as the “Alfvén surface”). A braking torque is applied because there is corotation out to some effective radius larger than the stellar radius and the net result is stellar spin-down (Parker 1958).

Another factor affecting the AML in this process is the effect of the magnetic field on the stellar wind. In the solar case, the magnetic field determines not only the large-scale distribution of the wind (blowing along open field lines), but it also determines its bimodal structure (Phillips et al. 1995; Lamers & Cassinelli 1999; Suzuki 2006; Wang & Sheeley 2006; Cranmer et al. 2007). We can then infer that the distribution of stellar winds in stars with hot coronae such as that of the Sun will be tightly related to the coronal magnetic field configuration. As a result, the mass loss and AML will also be influenced by the magnetic field structure and its surface distribution.

Doppler imaging and Zeeman–Doppler imaging (ZDI) observations of a large number of stars have revealed that stellar magnetic active regions, appear as dark spots (“spots” hereafter), can appear in all latitudes, including the polar regions (Strassmeier 1996, 2001; Donati & Collier Cameron 1997). There is also some observational evidence that the polar regions of active stars harbor bright coronal structures (e.g., Chung et al. 2004). In order to understand AML in stars it is then important to study the relation between the distribution of stellar magnetic fields and their AML.

Weber & Davis (1967, WD hereafter) have shown that for an idealized, spherically symmetric configuration, the loss of angular momentum by the wind can be written as

$$\dot{J} = \frac{3}{2} \Omega \dot{M} r_A^2, \quad (1)$$

where Ω is the rotation rate, \dot{M} is the mass loss rate, and r_A is the radius of the Alfvén surface. Based on WD’s model, a large number of more detailed and complex studies of AML in cool and hot stars, as well as in protostellar accretion disks, have been done both analytically (Mestel 1968; Holzwarth 2005) and numerically (Keppens & Goedbloed 2000; Matt & Pudritz 2008a, 2008b; Ud-Doula et al. 2009). In particular, Aibéo et al. (2007) have shown that AML can be modified by a factor of 2–4 when introducing magnetic flux at high latitudes. They explain the change in AML as a result of a change in the mass flux or the size of the Alfvén surface, but they argue that the change in the magnetic flux tubes topology should not significantly affect magnetic braking.

In all of the studies mentioned above, the wind distribution has been specified by some ad hoc assumptions, though with a strong physical basis, such as Parker’s wind solution. Such a “predefined” wind can be appropriate in the case of an idealized and simplified magnetic field topology, in which the steady-state wind structure can be predicted. Even the well known Parker solution, which provides a very good first order approximation for the solar wind, is hydrodynamic in nature and assumes an idealized, spherically symmetric field configuration, with the flow freely moving along open field lines. These studies are very useful for a parametric study of AML in stars, but they are similar to the potential field approximation (Altschuler & Newkirk 1969; McIvor et al. 2003; Donati 2008), in which strong assumptions about the boundary conditions have been made.

In order to compute AML in stars more realistically, one should calculate the true, nonspherical, Alfvén surface, as well as the actual wind distribution that results when realistic magnetic fields with higher degree of complexity (i.e., with star spots)

are introduced. In this work, we present an implementation of a global magnetohydrodynamic (MHD) model, originally developed for the solar corona (SC), to the corona of a Sun-like star. This model is driven by “realistic” surface magnetograms and it captures the detailed physics of the corona. Unlike other models, the wind in this model is determined by the magnetic field configuration in a self-consistent manner. We exploit this approach as a tool to investigate the effect of the magnetic field topology on the wind structure and AML in a more consistent and realistic way. In particular, we focus on the effect of variations in star spot location and magnetic field magnitude on the wind structure, mass loss, and AML rates.

The topic of this paper covers overlapping issues from both solar and stellar astrophysics, in which different terminology is sometime used to describe similar processes. Readers unfamiliar with numerical models for the SC should consult Cohen et al. (2007, 2008) for a more detailed description of the terminology employed here.

We describe the numerical model in Section 2 and present numerical tests and results in Section 3. In Section 4, we discuss the implications of the results over the long term in the context of stellar evolution, as well as for the short-term variations in the stellar magnetic field (the stellar cycle). We summarize our conclusions in Section 5.

2. MODEL DESCRIPTION

In order to simulate the corona of a Sun-like star, we use a global MHD model developed for the SC at the University of Michigan. We describe the model here briefly, and refer the reader to Cohen et al. (2007, 2008) for a more complete description, supporting observational data, referencing, and model validation. The model is based on the BATS-R-US generic MHD code (Powell et al. 1999) and it is part of the Space Weather Modeling Framework (SWMF; Tóth et al. 2005).

The model solves the set of MHD equations:

$$\begin{aligned} \frac{\partial \rho}{\partial t} + \nabla \cdot (\rho \mathbf{u}) &= 0, \\ \rho \frac{\partial \mathbf{u}}{\partial t} + \nabla \cdot \left(\rho \mathbf{u} \mathbf{u} + p + \frac{B^2}{2\mu_0} - \frac{\mathbf{B}\mathbf{B}}{\mu_0} \right) &= \rho \mathbf{g}, \\ \frac{\partial \mathbf{B}}{\partial t} + \nabla \cdot (\mathbf{u}\mathbf{B} - \mathbf{B}\mathbf{u}) &= 0, \\ \frac{\partial}{\partial t} \left(\frac{1}{2} \rho u^2 + \frac{1}{\gamma - 1} p + \frac{B^2}{2\mu_0} \right) \\ + \nabla \cdot \left(\frac{1}{2} \rho u^2 \mathbf{u} + \frac{\gamma}{\gamma - 1} p \mathbf{u} + \frac{(\mathbf{B} \cdot \mathbf{B}) - \mathbf{B}(\mathbf{B} \cdot \mathbf{u})}{\mu_0} \right) &= \rho(\mathbf{g} \cdot \mathbf{u}), \end{aligned} \quad (2)$$

which describe the conservation of mass, momentum, magnetic flux, and total energy. The equations are solved in a Cartesian grid with adaptive mesh refinement (AMR) capabilities, while the condition $\nabla \cdot \mathbf{B} = 0$ is maintained using the Eight Wave scheme (Powell et al. 1999). This SC model has widely been used to simulate the steady-state solar corona, as well as coronal mass ejections (CMEs; e.g., Cohen et al. 2008; Manchester et al. 2008).

2.1. Wind Powering in the Numerical Model

In order to mimic the stellar wind powering, we adopt a non-polytropic approach where $\gamma = C_p/C_v$ is not constant. Here C_p and C_v are the specific heats of the gas. γ is observed to be close to unity at the base of the SC, but it approaches the value 5/3

above 15–20 R_\odot (Totten et al. 1995). We can assume that the energy necessary to power the wind corresponds to this change in γ . We can also assume that this change in γ is larger for the fast wind and smaller for the slow wind. The end result is that with a proper choice of the three-dimensional distribution of γ , we can mimic the volumetric heating of the wind and obtain a steady-state MHD solution for the corona without introducing any heating functions.

In the solar case, we specify the distribution of γ in a way that is consistent with observations. By then using the empirical Wang–Sheeley–Arge (WSA) model (Wang & Sheeley 1990; Arge & Pizzo 2000), we also obtain a wind spatial velocity distribution that is consistent with the magnetic field distribution. The WSA model relates the magnetic flux tube expansion rate, f_s , to the final wind speed blowing along this tube. The higher the expansion is, the slower the wind that originates from the tube and vice versa. By using the WSA model as an input, we constrain our model to approach the empirical value of the wind speed.

The WSA model has been developed to predict the solar wind speed at 1 AU based on the potential field approximation and magnetogram data. The model converts the surface magnetic field data into a spherical distribution of the terminal solar wind speed by matching its parameters with solar wind data at 1 AU. We assume that the wind in Sun-like stars is not significantly different in its underlying physics from the solar case, in particular the relation between the expansion rate and the wind speed. In principle, the dependence of the wind speed on the expansion rate, f_s , could be fitted to stellar wind observations such as those presented by Wood et al. (2005).

We calculate the potential field and WSA coefficients in order to obtain the spherical distribution of the final wind speed. We assume conservation of energy along a streamline (Bernoulli integral) so we can relate the value of the speed at one end of the field line far from the Sun to the value of γ at the coronal base at the other end. If we assume that far from the Sun the total energy roughly equals the kinetic energy we can obtain the following equation:

$$\frac{u_{\text{wsa}}^2}{2} = \frac{\gamma_0}{[\gamma_0 - 1]} \frac{p_0}{\rho_0} - \frac{GM_\odot}{R_\odot}, \quad (3)$$

where G is the gravitational constant, and M_\odot and R_\odot are the solar mass and radius respectively, u_{wsa} is the speed obtained by the WSA model and p_0 , ρ_0 , and γ_0 are the surface values of the pressure, density, and γ , respectively. Since the boundary conditions for the pressure and density are assumed to be known, we can obtain the boundary conditions for γ . In the next step, we introduce a radial function of γ so its value changes from the surface value to a spherically uniform value of 5/3 at $r = 12.5 R_\odot$. Finally, we solve the MHD equations self-consistently with nonuniform γ until the wind solution converges.

We stress that this wind solution is determined by the magnetic field configuration. Therefore, any change in the field topology should change the wind structure in the same way that the magnetic field dictates the general structure of the coronal solution.

3. SIMULATION

In this work, we focus on the effect of star spot latitude on the AML through the stellar wind. We have examined five test cases with different surface distributions of the magnetic field and have

Table 1

The g_1^0 (Dipole) Component of the Magnetic Field Harmonic Expansion for Different Spot Colatitudes

Colatitude	No Spots	10	30	60	75
1 kG	5.0	3.8	4.4	5.99	7.035
200 G	5.0	4.76	4.89	5.22	5.4

calculated the three-dimensional steady state solution for each case. The first case is a 5 G dipolar field with no spots at all. The other cases are a 5 G dipolar field superimposed with five spot pairs on each hemisphere, where the spot pairs are located at $\phi_s = 36^\circ, 108^\circ, 180^\circ, 252^\circ, 324^\circ$ in longitude. In each test case, we modify the spots colatitude to be $\theta_s = 10^\circ, 30^\circ, 60^\circ, 75^\circ$. For each case, we use a spot magnetic field of 1 kG and then repeat the simulation using a 200 G field. The general description of the magnetic field for each latitudinal case can be written as

$$B(\theta, \phi) = B_d + \sum_{\phi_s} A \cdot e^{-[(\phi - \phi_s)^2 + (\theta - \theta_s)^2]/2.5^2 \cos \theta}, \quad (4)$$

where B_d is the 5 G dipolar field, A is the field strength required for a magnetic flux of 1 kG (or 200 G) in a spot area of $6.25 \cos \theta$ degrees, and the summation is over the longitudes, ϕ_s , for a particular latitude, θ_s . θ and ϕ are both in units of degrees. The magnetic flux here corresponds to the quantity that would be obtained from stellar magnetogram observations using ZDI.

The polarity of each spot pair compared to the large-scale dipole is matched to the observed polarity of the emerging flux on the Sun (Babcock 1961). This perfect alignment of the active region is probably not realistic, since differential rotation will cause one side of the spot to trail after the other one. Therefore, our three-dimensional simulation could be thought as a series of two-dimensional axial simulations.

In each case, the artificial magnetogram and potential field are calculated. Table 1 and Figure 1 show the g_1^0 (dipole) components for each case. It is clear that the dipole moment gets weaker for low latitude spots (less than 30°) while it gets stronger with high latitude spots. The potential field distribution serves as the initial condition for the magnetic field in our simulation. We then calculate the WSA speed distribution and the distribution of γ for each case. Finally, we run the MHD code until a steady state is obtained.

In all test cases, initial and boundary conditions are determined in the manner described by Cohen et al. (2007). We use a Cartesian grid with 10 levels of mesh refinement so that the grid cell size near the inner boundary is of the order of $1/200 R_*$, where R_* is the stellar radius. This high resolution is required in order to resolve the active region with at least several grid cells. We also dynamically refine the grid around current sheets that appear in the simulation. All MHD computations were performed using the Pleiades cluster at NASA's NAS center.

3.1. Wind Dependence on the Magnetic Field Structure

Figure 2 shows the surface radial magnetic field strength for each test case (left) and the resulting wind speed distribution calculated from the WSA model (right). It is obvious here that there is a strong dependence of the wind structure on the magnetic field topology. The main effect in the case of introducing strong spots on top of a dipolar field is that the fast wind gets eliminated as the spots migrate toward the pole. In the polar spot case, there is no fast wind at all except for two strips of moderate wind (500 km s^{-1}) at mid-latitudes, which is consistent with the study of McIvor et al. (2004).

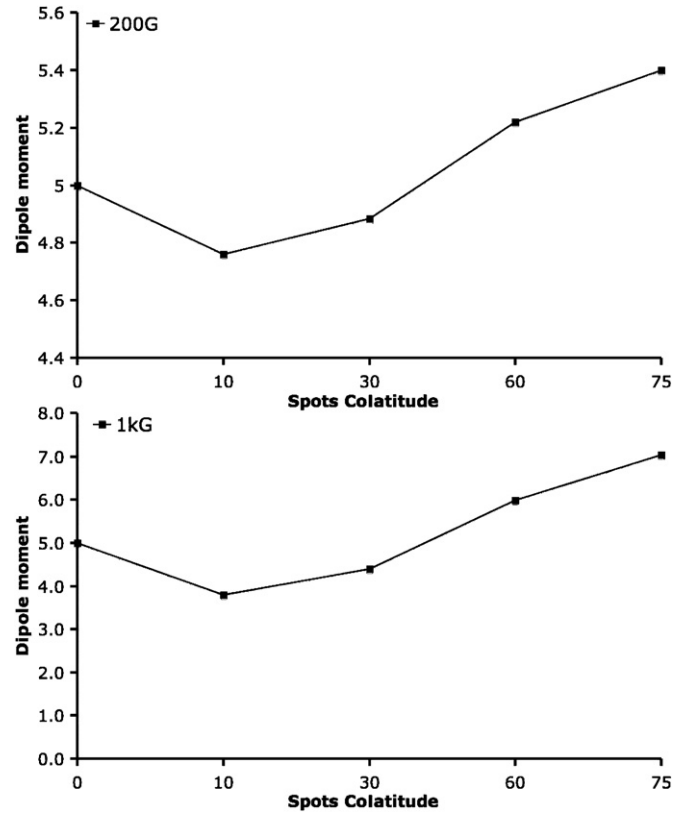


Figure 1. g_1^0 (dipole) component of the magnetic field harmonic expansion with spot strength of 200 G (top) and 1 kG (bottom) as a function of colatitude.

The reason for this behavior can be found by observing the detailed structure of the magnetic field in the vicinity of a star spot. Figure 3 shows the magnetic field topology near the star spot for the equatorial case (left) and the polar case (right). The surface is at $r = 1.04 R_*$, color contours are of radial field strength, and streamlines represent the three-dimensional magnetic field lines. The fast wind comes from open field regions, where the expansion of the flux tubes is small (Wang & Sheeley 1990). In the equatorial case, the star spots interact mostly with the closed streamers and only slightly with the open flux located at the coronal hole boundary. Therefore, there will be some closing of open field lines and a slight increase in the expansion of the tube, resulting in some removal of the fast wind. In the polar case, the star spots interact completely with field lines originally open, so that there are no longer regions with non-expanding flux tubes and the fast wind is completely eliminated. The regions with the minimum expansion are located at mid-latitude where we find moderate wind strips.

3.2. Mass and Angular Momentum Loss Rates

Once a steady state is obtained for each case, we calculate the Alfvénic Mach number, $M_A = u_{\text{SW}}/u_A$, with $u_A = B/\sqrt{4\pi\rho}$ being the Alfvén speed, and compute the Alfvén surface as that where $M_A = 1$. The mass loss rate through the wind, \dot{M} , can be calculated by integrating the mass flux through the Alfvén surface:

$$\dot{M} = \int \rho \mathbf{u} \cdot d\mathbf{a}_A, \quad (5)$$

where $d\mathbf{a}_A$ represents a surface element on the Alfvén surface. The mass flux does not depend of course on the particular surface of integration, since it is conserved.

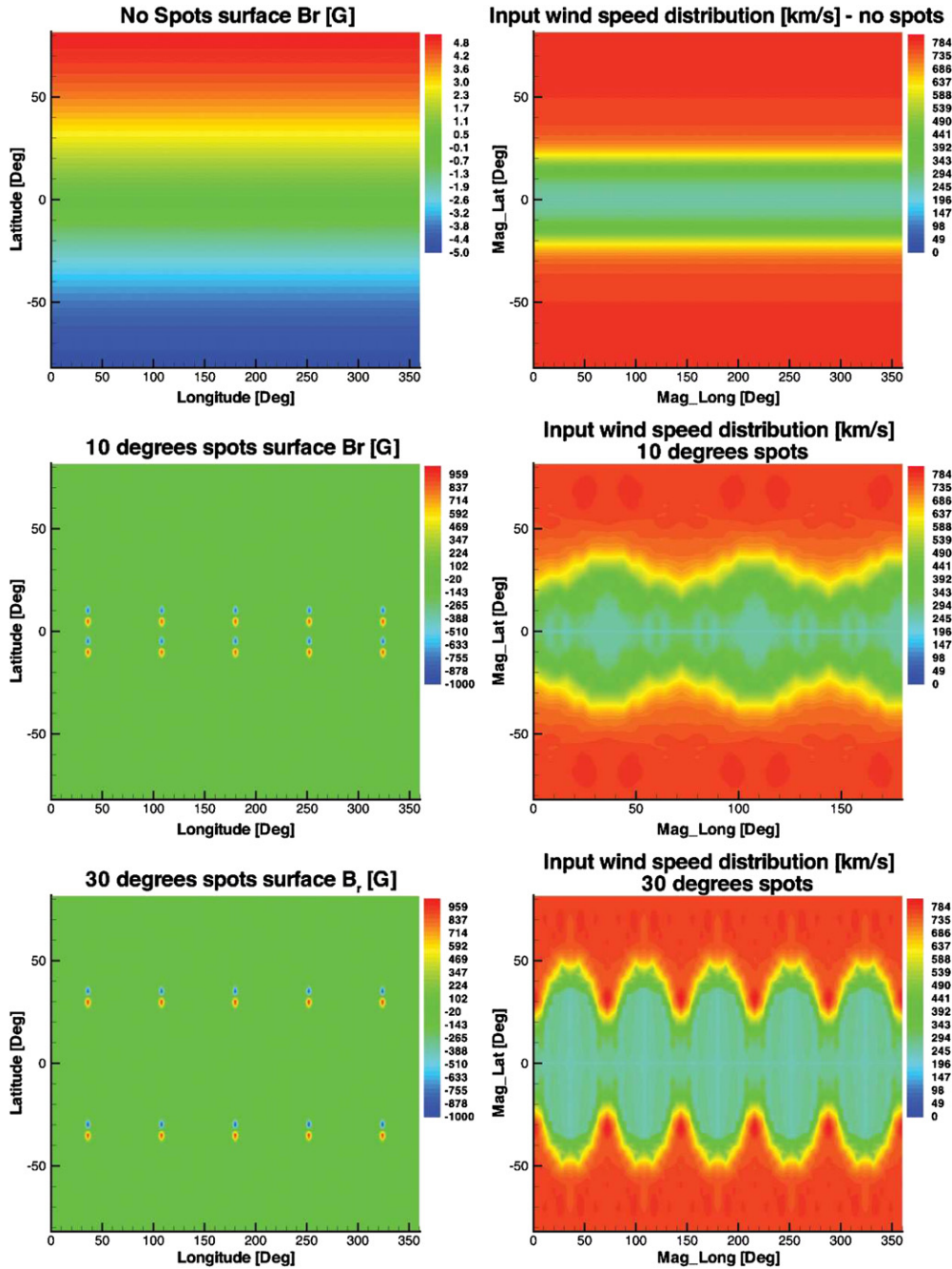


Figure 2. Surface radial field strength with color contours representing B_r [G] (left) and resulted input speed distribution calculated by the WSA model with color contours representing u_{WSA} (km s^{-1}) (right). The plots are for (top to bottom) dipolar field with no spots, and spots at 10° , 30° , 60° , 75° from the equator. (A color version and an extended version of this figure are available in the online journal.)

In a similar manner, the AML rate, \dot{J} , can be obtained using Equation (1):

$$\dot{J} = \frac{3}{2} \int \Omega \sin \theta r_A^2 \rho \mathbf{u} \cdot d\mathbf{a}_A, \quad (6)$$

where r_A and θ are the local radius and latitude at each element of the Alfvén surface.

The accuracy of the results depends mostly on the grid resolution. Since we use a nonuniform grid, we estimate the accuracy of our calculation for the largest grid cells on the Alfvén surface, assuming the result would be more accurate

where smaller grid cells used. We found that for the largest grid cells $\Delta \dot{M} / \dot{M} \leq 0.001$ and $\Delta \dot{J} / \dot{J} \leq 0.1$.

3.3. Results for the Case of 1 kG Spots

Figure 4 shows the $y = 0$ plane from the three-dimensional steady-state solution for each test case (top to bottom). The color contours are of number density (left) and radial wind speed (right). Black streamlines in each panel represent the magnetic field lines, while the solid white line represents the Alfvén surface. The left–right asymmetry is due to the fact that the cut goes through the spots on the left side, while it goes between two spots on the right side.

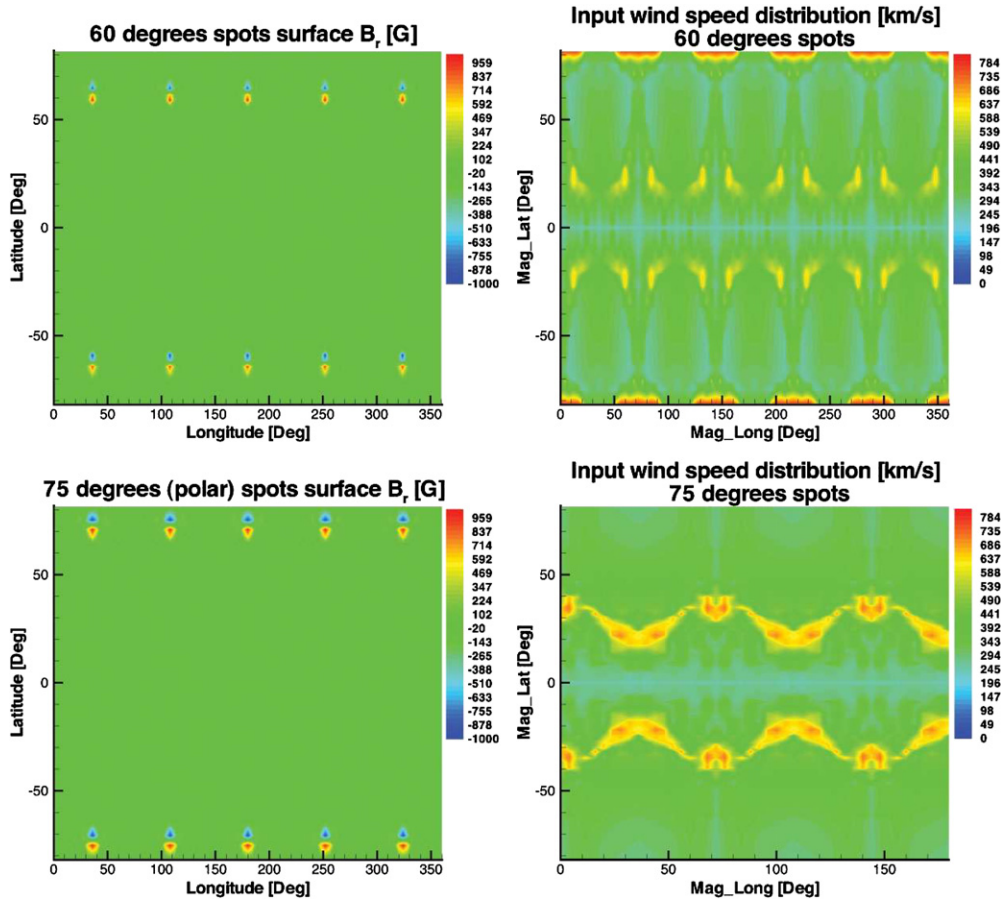


Figure 2. (Continued)

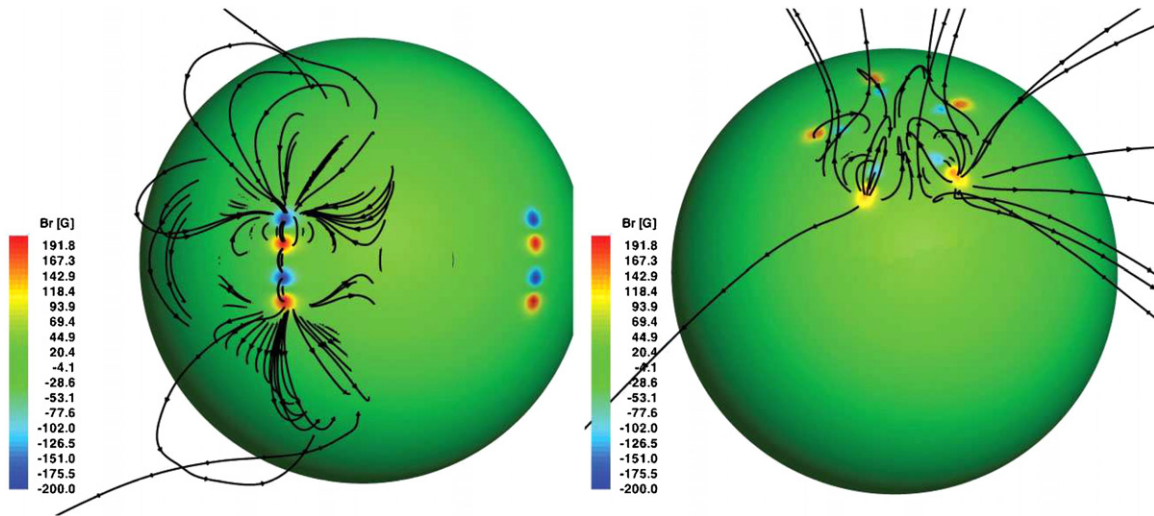


Figure 3. Star spots located at 10° from the equator (left) interact mostly with the closed field streamers, while polar spots located at 80° (right) interact mostly with open flux. The sphere is of $r = 1.04 R_*$, so B_r of the spots is weaker than the surface value.

(A color version and an extended version of this figure are available in the online journal.)

The existence of the strong magnetic field from the spots locates the Alfvén surface in this direction further out at larger radial distance than in the pure dipolar field case. Another consequence of the increase in magnetic field strength due to the strong spots is that the current sheet is wider than that in the dipolar case.

The results of the MHD solution are consistent with the input speed distribution obtained by the WSA model, and the figures show how the fast wind is being eliminated as the spots migrate

toward the pole. As the spots move toward the pole, the Alfvén surface shrinks and is smallest in the case of 60° colatitude. The Alfvén surface gets bigger for the polar case, since the field strength at high latitudes on the surface is higher due to the polar spots. In addition, the overall slowdown in the wind for more poleward spots causes the density to increase, so we find a significant increase in the total mass within the corotating volume between the surface of the star and the Alfvén surface.

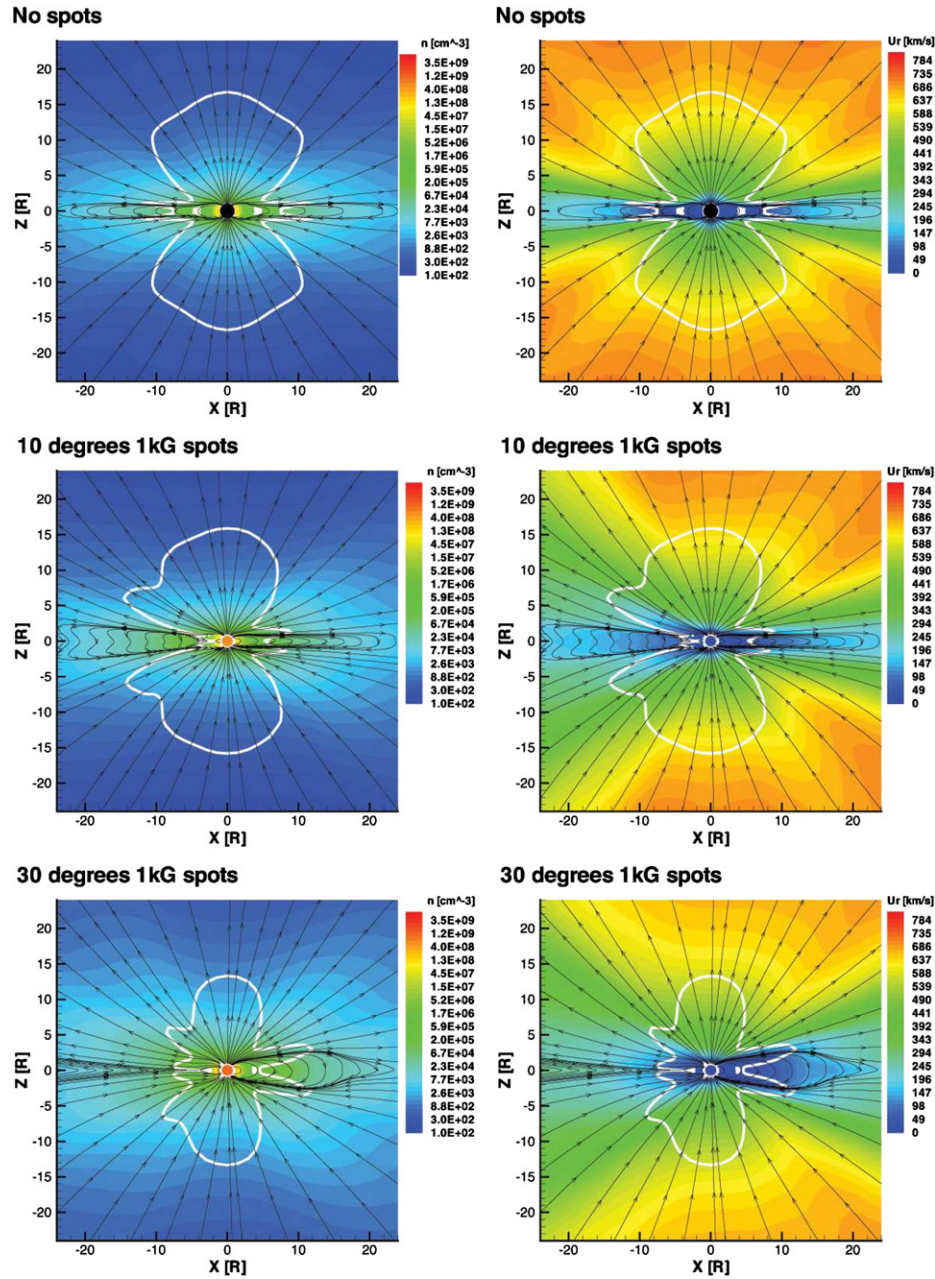


Figure 4. A $y = 0$ cuts in the three-dimensional steady state solutions contain 1 kG spots. Top to bottom show the no spots case and the cases in which the spots are located at the colatitudes of 10° , 30° , 60° , and 75° . Color contours are of number density (left) and radial wind speed (right). Streamlines represent the magnetic field lines, the white solid line represents the Alfvén surface.

(A color version and an extended version of this figure are available in the online journal.)

3.4. Results for the Case of 200 G Spots

Figure 5 shows the simulation results with spot magnetic fields of 200 G. It can be seen for this weaker field that the effect of fast wind elimination is reduced due to the correspondingly weaker interaction of the spot and ambient fields. Unlike the 1 kG case for 60° and 75° , in which wind over $300\text{--}400\text{ km s}^{-1}$ has been completely eliminated, in the 200G case there is still some faster wind at higher latitudes.

4. DISCUSSION

4.1. The Effect of Wind Distribution on AML

Figure 6 shows line plots of mass loss rate (top) and AML rate (bottom), denoted by dM and dJ , as a function of spot

colatitude for the 1 kG case (squares) and the 200G case (triangles). The rates are normalized to the mass loss rate $dM_0 = 1.5 \times 10^{-14} M_\odot \text{ yr}^{-1}$, and the AML rate $dJ_0 = 10^{30} \text{ g cm}^2 \text{ s}^{-2}$, of the dipolar case. dM_0 is also consistent with the solar mass loss rate calculated using typical solar wind parameters at 1 AU (e.g., Gombosi 2004).

The loss rates depend on the interplay between the wind speed, density, and the size of the Alfvén surface. In principle, one should expect the AML rate to be controlled mainly by the mass flux. However, this seems to be true only when the fast wind dominates, as in the dipolar case or when the spots are near the equator.

In the dipole field case with no spots, the rates depend on the high mass flux due to the fast wind at high latitudes, and on the relatively high density and stronger magnetic field close

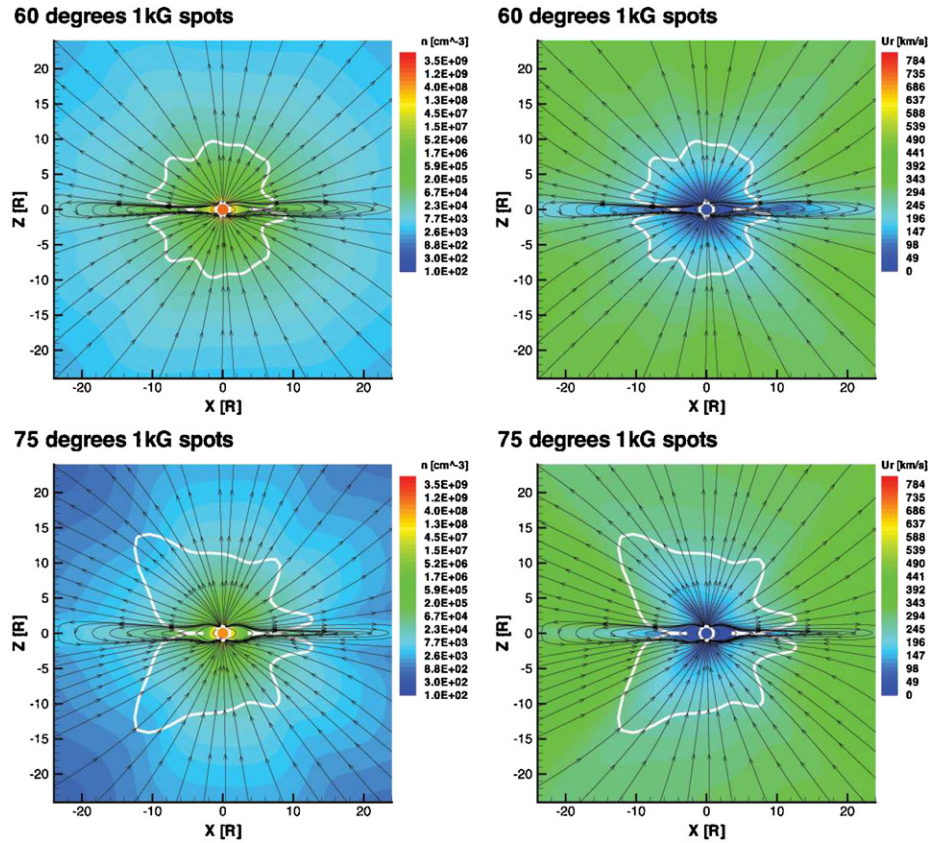


Figure 4. (Continued)

to the equator. When introducing equatorial spots, they interact with the closed field streamers so the density structure near the current sheet does not change much. In this case, the equatorial effects on the loss rates are not significantly different and the AML rate is controlled by the change in the mass flux.

When the spots are located at higher latitudes the amount of fast wind is decreased and the AML is actually affected most by the significant increase in density in the volume between the stellar surface and the Alfvén surface. It is possible that this high density, slow wind is related to the accumulation of $H\alpha$ -emitting gas in “slingshot” prominences now commonly observed on rapidly rotating stars (Collier Cameron & Robinson 1989; Collier Cameron & Woods 1992; Jeffries 1993; Byrne et al. 1996; Eibe 1998; Donati et al. 2000; Jardine & van Ballegooijen 2005). The star tries to corotate the plasma that exists between its surface and the Alfvén surface, but the stronger field and higher plasma mass density apply more torque on the star. The net result is higher loss of angular momentum, which in this case might be described as AML to the stellar outer atmosphere rather than the stellar wind. The mass flux is higher for the case of polar spots with 200 G than for just the dipole (as seen at the top of Figure 6), and the net AML is still greater for the case of 1 kG spots (as seen at the bottom of Figure 6). Figure 7 shows a cartoon of the effect of spot location on AML.

The overall trend in Figure 5 inverts below 10° due to the size of the Alfvén surface. In the case of 1 kG spots, more fast wind is eliminated and the Alfvén surface is expanded, so the total mass flux and AML are lower. In the case of 200 G spots, the Alfvén surface is smaller than the case with no spots. While in this case the wind distribution is similar to the no spots case, the Alfvén surface is now located in regions of higher density so the total mass flux through the surface is higher.

4.2. Implications for the Long-term Stellar Evolution

The appearance of polar spots in fast rotating stars has been explained by the enhancement of Coriolis force acting on the emerging flux tubes (Schuessler & Solanki 1992) or alternatively by the behavior of the meridional circulation in fast-rotating stars (Schrijver & Title 2001). In both cases, the rotation rate affects the magnetic field distribution. Aibéo et al. (2007) have argued that redistribution of the coronal flux in stars does not significantly change the wind efficiency for the magnetic breaking. However, their model took into account only the existing magnetic flux with no addition of new emerging flux (i.e., active regions or spots). Our results clearly show that the AML through the wind is affected by the location, as well as the strength, of the spots. Therefore, we argue that as a result of fast-rotating young stars having their new magnetic flux appear in high latitudes, their winds are organized in such a way that the AML and the spin down of the star are large. As the rotation rate decreases, the new magnetic flux appears at lower latitudes and consequently the wind is organized in a way that the AML decreases as well.

The aim of our study is to begin to understand how AML changes with surface magnetic topology, with the ultimate aim of understanding the rotational evolution of stars. On more magnetically active stars, we expect the strength of the spots, as well as the strength of the background dipole, to be higher than the Sun-like case. The stronger surface field will induce a stronger stellar wind, so the “ambient” mass-loss and AML rates from these stars would be higher, regardless of the magnetic spot distribution. Here, we have examined how redistributing the surface field affects the stellar wind distribution and its AML. The dominant effect we found was the reorganization

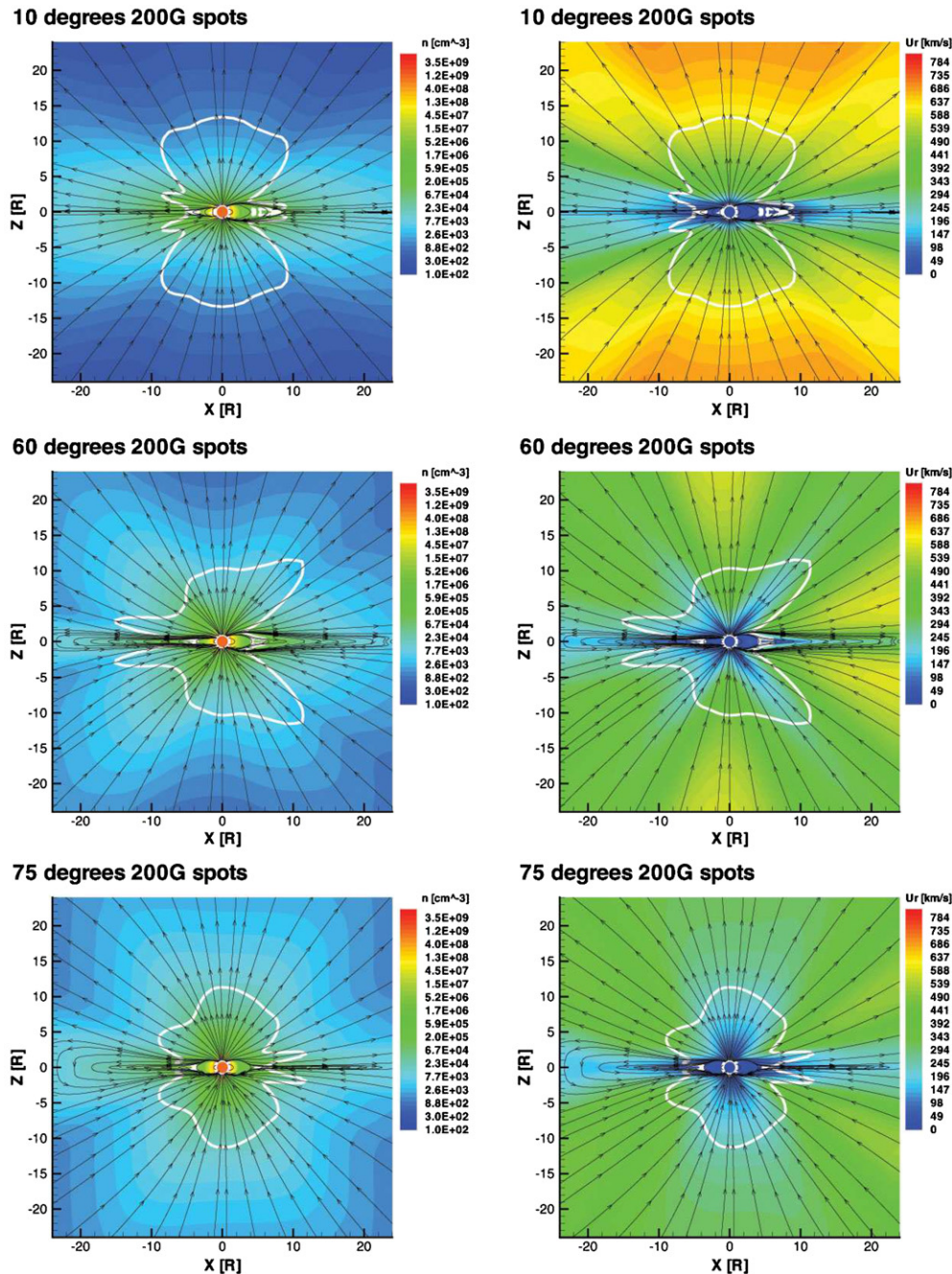


Figure 5. A $y = 0$ cuts in the three-dimensional steady state solutions contain 200G spots. Top to bottom show the cases in which spots are located at colatitudes of 10° , 60° , and 75° . Display is the same as Figure 3.
(A color version and an extended version of this figure are available in the online journal.)

of the open/closed field lines for the different spot latitudes, and elimination of the fast wind for high latitude spots. As the strength of the dipole is increased, the influence of the spots on the magnetic field distribution will be diminished. For a very strong background dipole an order of magnitude or more higher than considered here, the effect of the spots is likely to be quite small. It is not yet known how the dipolar field scales with stellar activity in general, and future theoretical investigation of the effects of the dipolar field strength on AML would be worthwhile.

Kawaler (1988) developed a general expression for the rotational evolution of low-mass stars based on the WD formalism

(Equation (1)) and an assumed linear scaling of radial and dipolar surface magnetic field strength with rotation rate, $B_0 \propto \Omega$. This simple type of approach has proven to be reasonably successful at matching stellar rotation velocities versus age for solar-like stars of Hyades age (600 Myr) and older (e.g., Kawaler 1988; Krishnamurthi et al. 1997; Sills et al. 2000). However, the relation fails for earlier ages because the predicted AML is too high to explain rapid rotators with periods of one to several days in younger open cluster stars (e.g., Stauffer et al. 1987; Barnes & Sofia 1996; Krishnamurthi et al. 1997). To avoid this problem, Krishnamurthi et al. (1997) introduced a “saturation” in the dependence of the surface magnetic field on rotation

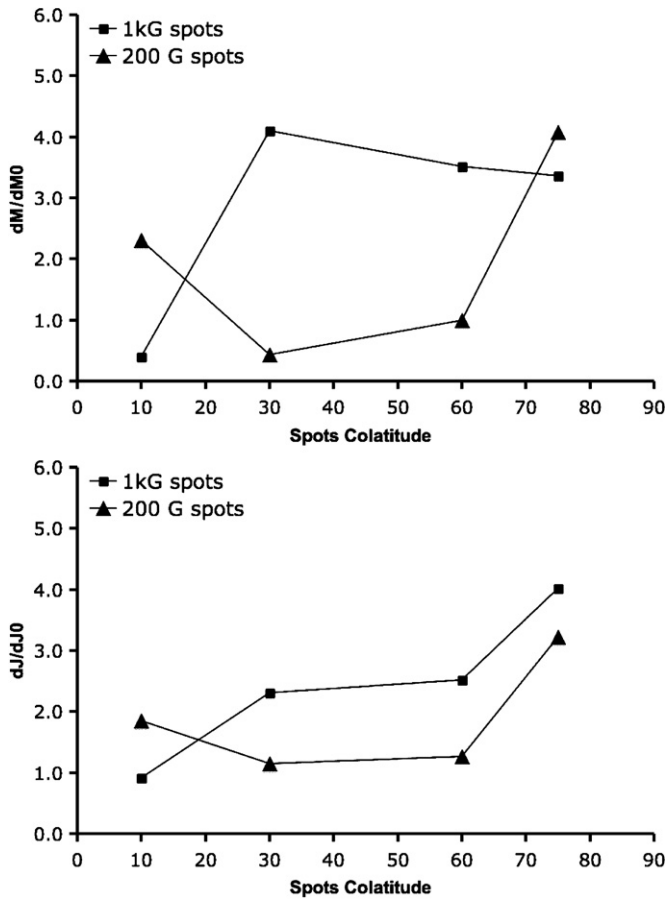


Figure 6. Line plot of mass (top) and AML (bottom) rates denoted by dM and dJ as a function of spots colatitude for 1 kG spots (squares) and 200G spots (triangles). Rates are normalized to the loss rates of the dipolar case dM_0 and dJ_0 .

rate: beyond some critical period the surface field was assumed constant.

Rotation periods of one to several days also represent the regime in which high-latitude surface spots are observed in single and tidally locked binaries (e.g., Strassmeier 2001). It is in this regime that the complications of spot latitude on AML discussed here will be important. The results indicate that a simple saturation of the dynamo itself and the representation of the surface field through a mixture of radial and dipole components is likely to be an inadequate description. Such oversimplification might also confuse the division between wind AML and internal angular momentum redistribution that is thought significant at ages younger than those of the Hyades (Sills et al. 2000). Disentangling these effects is likely to require both sophisticated dynamo and stellar structure models, in addition to coronal MHD wind models such as those presented here. However, much empirical progress could still be made through the application of the latter models to stellar surface magnetograms for stars with different rotation periods in order to probe the nonorthogonal interplay between magnetic field configuration and AML.

4.3. Implications for the Short Term Stellar Evolution and Stellar Dynamos

One can ask whether there might be a feedback mechanism between the rotation, AML and the magnetic field structure. It has been shown that redistribution of stellar magnetic fields

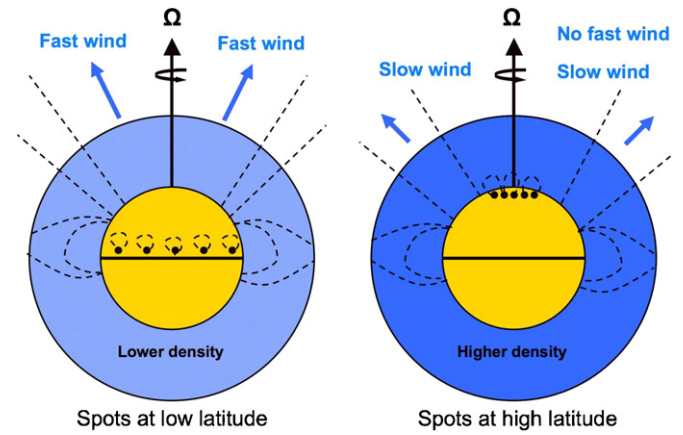


Figure 7. Effect of spot location on the AML. The inner circle represents the star and the outer circle represents the Alfvén surface with tentative field lines (dashed lines). The left panel shows the case of low-latitude spots, in which the AML is controlled by the high mass loss through the fast wind at high latitudes. In the right panel, which shows the situation for high-latitude strong spots, the fast wind is eliminated and so does the high mass loss at high latitudes. As a result, the total density in the volume is high and applies more torque on the star due to the imperfect corotation and the fact that it is frozen-in to the magnetic field.

(A color version of this figure is available in the online journal.)

affects the spin down of stars and reduces their necessity for dynamo saturation (Solanki et al. 1997; Holzwarth & Jardine 2005). Our results take a step forward in this approach. We suggest that variations in the the spot latitudes redistribution of the surface magnetic field can lead to variations in the wind distribution (as observed in the solar case) and as a result, the AML is modified. If the variations of the AML affect the motions generating the new magnetic flux (i.e., the convection zone) through small variations of the rotation rate, then we speculate that this might be the connection between the corona and the stellar cycle.

Nevertheless, the feedback from the coronal magnetic field on the solar dynamo has not been studied in detail yet. It is possible to perform angular momentum and mass loss rates calculations based on the same method described in this paper, but driven by real solar magnetogram data. The predicted variations in AML and mass-loss should be compared with variations of rotation rates in the convection zone measured by GONG and MDI (e.g., Antia et al. 2008).

5. CONCLUSIONS

We test the effect of star spot latitudinal location and magnetic field strength on stellar AML via the stellar wind. Unlike previous studies, we use a model in which the wind distribution is dictated by the magnetic field structure. This key feature is crucial in order to get a more realistic picture of the corona, in particular in terms of the AML rate. Even though we use a solar-like wind distribution in this work, it seems likely that the relationship between the solar magnetic field expansion and the solar wind is universal and can be applied to other Sun-like stars.

We find that the change in magnetic field structure significantly affects the wind structure and as a result, the loss of angular momentum. In particular, we find that the AML rate is controlled by the mass flux when spots are located at low latitudes. When spots are located at high latitudes however, the AML rate is controlled by the density increase as a result of fast wind elimination.

This work is a step further in our understanding of the role of magnetic fields in stellar evolution, stellar dynamos, and stellar coronal structure. A further investigation of these topics involving MHD solutions driven by surface field maps of real stellar systems (e.g., Hussain et al. 2007; Gregory et al. 2008), as well as further study of idealized cases such as the work presented here, could be of great interest. This work also demonstrates how the detailed knowledge of the physics of the solar corona can be implemented for other stars as we study the solar–stellar connection.

We thank the anonymous referee for useful comments and suggestions. This work has been supported by NSF-SHINE ATM-0823592 grant, NASA-LWSTRT Grant NNG05GM44G. Simulation results were obtained using the Space Weather Modeling Framework, developed by the Center for Space Environment Modeling, at the University of Michigan with funding support from NASA ESS, NASA ESTO-CT, NSF KDI, and DoD MURI. J.J.D. and V.L.K. were funded by NASA contract NAS8-39073 to the *Chandra* X-ray Center (CXC) during the course of this research.

REFERENCES

- Aib  o, A., Ferreira, J. M., & Lima, J. J. G. 2007, *A&A*, **473**, 501
- Altschuler, M. D., & Newkirk, G. 1969, *Sol. Phys.*, **9**, 131
- Antia, H. M., Basu, S., & Chitre, S. M. 2008, *ApJ*, **681**, 680
- Arge, C. N., & Pizzo, V. J. 2000, *J. Geophys. Res.*, **105**, 10465
- Babcock, H. W. 1961, *ApJ*, **133**, 572
- Barnes, S., & Sofia, S. 1996, *ApJ*, **462**, 746
- Byrne, P. B., Eibe, M. T., & Rolleston, W. R. J. 1996, *A&A*, **311**, 651
- Chung, S. M., Drake, J. J., Kashyap, V. L., Lin, L. W., & Ratzlaff, P. W. 2004, *ApJ*, **606**, 1184
- Cohen, O., Sokolov, I. V., Roussev, I. I., & Gombosi, T. I. 2008, *J. Geophys. Res. (Space Physics)*, **113**, 3104
- Cohen, O., et al. 2007, *ApJ*, **645**, L163
- Collier Cameron, A., & Robinson, R. D. 1989, *MNRAS*, **236**, 57
- Collier Cameron, A., & Woods, J. A. 1992, *MNRAS*, **258**, 360
- Cranmer, S. R., van Ballegoijen, A. A., & Edgar, R. J. 2007, *ApJS*, **171**, 520
- Donati, J.-F. 2008, in ASP Conf. Ser. 384, 14th Cambridge Workshop on Cool Stars, Stellar Systems, and the Sun, ed. G. van Belle (San Francisco, CA: ASP), 156
- Donati, J.-F., & Collier Cameron, A. 1997, *MNRAS*, **291**, 1
- Donati, J.-F., Mengel, M., Carter, B. D., Marsden, S., Collier Cameron, A., & Wichmann, R. 2000, *MNRAS*, **316**, 699
- Eibe, M. T. 1998, *A&A*, **337**, 757
- Gombosi, T. I. 2004, *Physics of the Space Environment* (ISBN 052160768X; Cambridge: Cambridge Univ. Press)
- Gregory, S. G., Matt, S. P., Donati, J.-F., & Jardine, M. 2008, *MNRAS*, **389**, 1839
- Holzwarth, V. 2005, *A&A*, **440**, 411
- Holzwarth, V., & Jardine, M. 2005, *A&A*, **444**, 661
- Hussain, G. A. J., et al. 2007, *MNRAS*, **377**, 1488
- Ivanova, N., & Taam, R. E. 2003, *ApJ*, **599**, 516
- Jardine, M., & van Ballegoijen, A. A. 2005, *MNRAS*, **361**, 1173
- Jeffries, R. D. 1993, *MNRAS*, **262**, 369
- Kawaler, S. D. 1988, *ApJ*, **333**, 236
- Keppens, R., & Goedbloed, J. P. 2000, *ApJ*, **530**, 1036
- Krishnamurthi, A., Pinsonneault, M. H., Barnes, S., & Sofia, S. 1997, *ApJ*, **480**, 303
- Lamers, H. J. G. L. M., & Cassinelli, J. P. 1999, *Introduction to Stellar Winds* (Cambridge: Cambridge Univ. Press)
- Manchester, IV, W. B., et al. 2008, *ApJ*, **684**, 1448
- Matt, S., & Pudritz, R. E. 2008a, *ApJ*, **678**, 1109
- Matt, S., & Pudritz, R. E. 2008b, *ApJ*, **681**, 391
- McIvor, T., Jardine, M., Cameron, A. C., Wood, K., & Donati, J.-F. 2003, *MNRAS*, **345**, 601
- McIvor, T., Jardine, M., Cameron, A. C., Wood, K., & Donati, J.-F. 2004, *MNRAS*, **355**, 1066
- Mestel, L. 1968, *MNRAS*, **138**, 359
- Parker, E. N. 1958, *ApJ*, **128**, 664
- Phillips, J. L., et al. 1995, *Geophys. Res. Lett.*, **22**, 3301
- Powell, K. G., Roe, P. L., Linde, T. J., Gombosi, T. I., & De Zeeuw, D. L. 1999, *J. Comput. Phys.*, **154**, 284
- Schrijver, C. J., & Tittle, A. M. 2001, *ApJ*, **551**, 1099
- Schuessler, M., & Solanki, S. K. 1992, *A&A*, **264**, L13
- Sills, A., Pinsonneault, M. H., & Terndrup, D. M. 2000, *ApJ*, **534**, 335
- Solanki, S. K., Motamen, S., & Keppens, R. 1997, *A&A*, **324**, 943
- Stauffer, J. R., Hartmann, L. W., & Latham, D. W. 1987, *ApJ*, **320**, L51
- Strassmeier, K. G. 1996, in IAU Symp. 176, *Stellar Surface Structure*, ed. K. G. Strassmeier & J. L. Linsky (Dordrecht: Kluwer), 289
- Strassmeier, K. G. 2001, in ASP Conf. Ser. 223, 11th Cambridge Workshop on Cool Stars, Stellar Systems and the Sun, ed. R. J. Garcia Lopez, R. Rebolo, & M. R. Osorio Zapaterio (San Francisco, CA: ASP), 271
- Suzuki, T. K. 2006, *ApJ*, **640**, L75
- T  th, G., et al. 2005, *J. Geophys. Res.*, **110**, A12226
- Totten, T. L., Freeman, J. W., & Arya, S. 1995, *J. Geophys. Res.*, **100**, 13
- Ud-Doula, A., Owocki, S. P., & Townsend, R. H. D. 2009, *MNRAS*, **392**, 1022
- Wang, Y.-M., & Sheeley, N. R. 1990, *ApJ*, **355**, 726
- Wang, Y.-M., & Sheeley, Jr, N. R. 2006, *ApJ*, **653**, 708
- Weber, E. J., & Davis, L. J. 1967, *ApJ*, **148**, 217
- Wood, B. E., M  ller, H.-R., Zank, G. P., Linsky, J. L., & Redfield, S. 2005, *ApJ*, **628**, L143